Autonomous Development of Compositional Diversity in Self-Spreading Flat Protocells

ChemSystemsChem

Research Article
doi.org/10.1002/syst.202400029

Chemistry Europe
European Chemical Societies Publishing

www.chemsystemschem.org

Autonomous Development of Compositional Diversity in Self-Spreading Flat Protocells

İrep Gözen,*[a] Stephen Mann,[b] and Aldo Jesorka[c]

An experimental pathway to the spontaneous generation of compositionally diverse synthetic protocells is presented. The pathway is initiated by flat giant unilamellar vesicles (FGUVs) that originate from compositionally different multilamellar lipid reservoirs and undergo spontaneous spreading across solid surfaces. On contact, the spreading FGUVs merge to produce a concentration gradient in membrane lipids across the fusion interface. Subsequent reconstruction through a series of shape transformations produces a network of nanotube-connected lipid vesicles that inherit different ratios of the membrane constituents derived from the bilayers of the parent FGUVs. The fusion process leads to the engulfment of small FGUVs by larger FGUVs, mimicking predator-prey behavior in which the observable characteristics of the prey are lost but the constituents are carried by the predator FGUV to the next generation of lipid vesicles. We speculate that our results could provide a feasible pathway to autonomous protocell diversification in origin of life theories and highlight the possible role of solid surfaces in the development of diversity and rudimentary speciation of natural protocells on the early Earth.

Introduction

Evolutionary processes of selection and gradual optimization in structure and function amongst diverse cellular entities are considered key driving forces leading to the complexity of living organisms. Back-extrapolation of these mechanisms to the emergence of prebiotic cells on the early Earth before the advent of genotype/phenotype correlations is challenging given that the unsophisticated structure and limited functions of natural protocells would seemingly not support the gradual development of diversity and speciation required for Darwinian selection.[1] While concepts of natural protocell competition and heredity have been theoretically discussed,[2] the properties responsible for the possible differentiation of prebiotic cells into different non-genetic lineages remain unknown. In principle, the demarcation of primitive cells into functionally identifiable populations could be based on differences in the interplay of certain physical characteristics with the environment. For example, rudimentary forms of diversity could be generated by groupings based on differences in protocell size and attendant changes in surface energy, elasticity, porosity and permeability[3] that generate selection pressures and thereby optimize survival in different local environments. Alternatively, lineages based on compositional diversity could be generated by compartmentalization and self-maintenance of distinct chemical sets of constituents such as primitive peptides and catalysts.[1b]

At the most primitive level, sub-sets of prebiotic cells with the same internal constituents could be envisaged solely based on their variability in membrane composition. Given that such a scenario could represent a basal condition for the onset of diversity, quasi-speciation and non-genetic inheritance of natural protocells on the early Earth, herein we develop an interactive protocell model capable of autonomously displaying compositional diversity in membrane composition. Specifically, we present experimental evidence showing that compositionally diverse sets of model protocells arise spontaneously through solid surface-supported self-optimization processes involving the attachment, self-spreading and interfacial mixing of flat giant unilamellar vesicles (FGUVs) generated from localized reservoirs of multilamellar phospholipid vesicles (MLVs).[4] Single FGUVs are produced by spontaneous self-spreading of an MLV, i.e. a lipid micro-droplet, upon contact with a high energy solid surface, such as silica or a metal oxide (Figure 1). MLVs arise spontaneously when dry layers of lipids are hydrated and can consist of tens to hundreds of lipid lamella interconnected through structural defects (Fig 1 A).[5] Upon contact with the solid surface, a double lipid bilayer emerges from each MLV and spreads isotropically on the surface (Figure 1A–B). Significantly, the surface-adhered double bilayer is an intact nanoscale compartment on the order of femtoliters in volume.[4a] The FGUVs are delineated by a fluid soft-matter flexible boundary capable of encapsulating molecular species and nanoparticles.[6] The viscosity of water confined between the supported membrane and substrate is considered to be 10^4 times higher than bulk water,[7] which enables the proximal (lower bilayer with respect to the solid surface) and

[a] Dr. İ. Gözen
Centre for Molecular Medicine Norway, Faculty of Medicine, University of Oslo, 0318 Oslo, Norway
E-mail: irep@uio.no

[b] Prof. S. Mann
Max Planck-Bristol Centre for Minimal Biology and Centre for Protolife Research, School of Chemistry, University of Bristol, Bristol BS8 1TS, UK

[c] Prof. A. Jesorka
Department of Chemistry and Chemical Engineering, Chalmers University of Technology, Göteborg SE-412 96, Sweden

Supporting information for this article is available on the WWW under https://doi.org/10.1002/syst.202400029

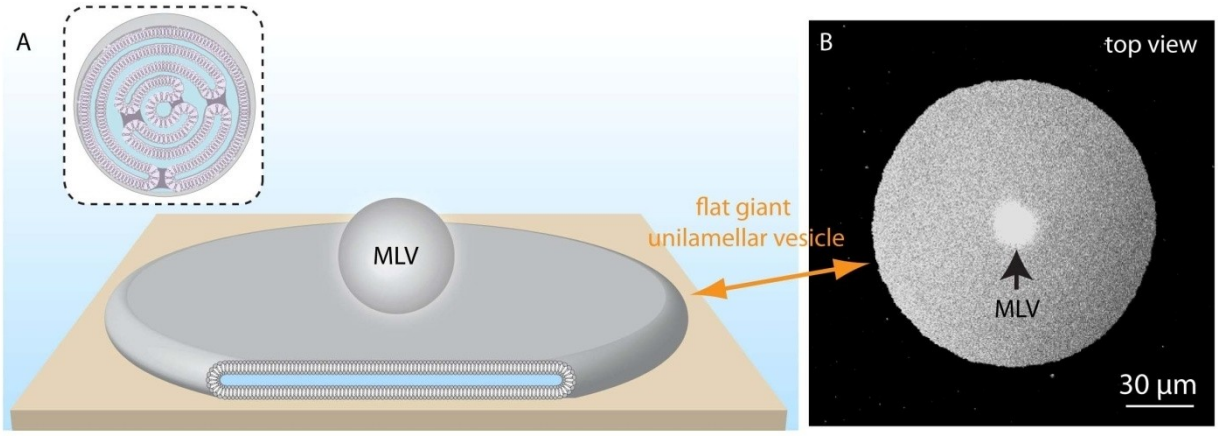

Figure 1. Flat giant unilamellar vesicles as a protocell model. (A) Schematic showing a cross section, i.e. side view, of a flat giant unilamellar vesicle (FGUV) produced by the self-spreading of a lipid reservoir consisting of a multilamellar vesicle (MLV) on a solid substrate (not to scale). The inset to (A) schematically depicts the internal structure of a MLV containing inter-bilayer defects.[5] (B) Confocal fluorescence micrograph, i.e. top view, of a surface-adhered FGUV with a MLV droplet reservoir (bright central region). 1 wt% of lipids in the membrane are chemically conjugated to a fluorophore (Texas Red DHPE) to enable imaging.

distal (upper bilayer with respect to the solid surface) membranes of the FGUVs to have different dynamic features. Connection of FGUVs to the MLV reservoir is maintained during spreading by a continuous supply of lipid molecules that helps balance the membrane tension of the FGUV. Consequently, the FGUV membrane remains attached throughout unlike conventional GUVs that are mostly suspended in bulk.[8] Overall, the spreading process is surface-specific. For example, reducing the surface energy by decreasing the concentration of divalent ions in the environment leads to reversible FGUV adhesion and detachment of surface-adhered membrane regions from the solid surface, resulting in retraction of the lipid material back into the reservoir[9] or transformation of the surface-detached membrane regions into spherical unilamellar vesicles.[10] On some surfaces, e.g. glass, the most outer bilayer shell of the MLV can immediately rupture, resulting in single bilayer spreading and formation of a supported lipid bilayer patch, which is a planar structure without an enclosed liquid volume.

In this paper, we exploit FGUVs as a dynamically interactive protocell model with unusual self-propelling properties that facilitate two-dimensional (2D) fusion, spatiotemporal changes in membrane reorganization and compositional diversity in next-generation vesicles. We show that self-spreading FGUVs with different lipid bilayer membrane compositions spontaneously fuse on contact, and through a series of consecutive shape deformations, transform into a network of nanotube-connected lipid vesicles. The merged protocells, nanotubes and next-generation vesicles comprise different ratios of the membrane constituents of the original FGUVs, establishing a defined protocell composition gradient with respect to the distance from the initial fusion interface. The composition gradient is determined by the geometry of the fusion interface, the ratio of the sizes of the fusing FGUVs, and the number of fusing FGUVs. Large FGUVs completely engulf smaller FGUVs, giving rise to artificial predator-prey behavior. Significantly, the 'phenotype' of the small FGUVs (prey) is lost on fusion, but its composition is inherited by the large FGUV (predator) as part of the next generation of lipid compartments produced after shape transformation. Our experimental findings reveal a feasible pathway leading to a rudimentary type of protocell diversity and speciation based on the two-dimensional (2D) fusion of self-spreading unilamellar lipid vesicles.

Results

Membrane Fusion and Mixing in Spreading Protocells

To establish the autonomous development of compositional diversity in dynamically interacting model protocells, we prepared FGUVs with different membrane compositions and allowed the spreading protocells to spontaneously merge as they advanced across a solid substrate (cf. SI section 1 for details of vesicle and surface preparation). Specifically, we used two types of MLV lipid reservoirs comprising 50 and 49 wt% of soy and *E. coli* polar lipid extracts, respectively, and 1 wt% of either (1,2-dioleoyl-sn-glycero-3-phosphoethanolamine-N-carboxyfluorescein (CF 488-DOPE, yellow fluorescence) or ATTO 655–1,2-dioleoyl-sn-glycero-3-phosphoethanolamine (ATTO 655-DOPE, magenta fluorescence). The MLV droplets were deposited on a flat SiO_2 surface submerged in an aqueous environment containing 4 mM Ca^{2+}. On physical contact with the surface at random locations the MLVs spontaneously spread towards each other, followed by collision and fusion (Figure 2A–B, SI Movie 1). The contact edges performed a tank-tread motion[11] (Figure 2B) as the bilayer membranes of the two flat protocells spontaneously merged, giving rise to diffusive mixing of their membrane lipids and aqueous contents (Figure 2C–D). The spontaneous merging of two FGUVs is energetically favorable because the line tension at the spreading front is reduced during this process. Line tension is caused by the high curvature at the perimeter of the FGUV. In contrast,

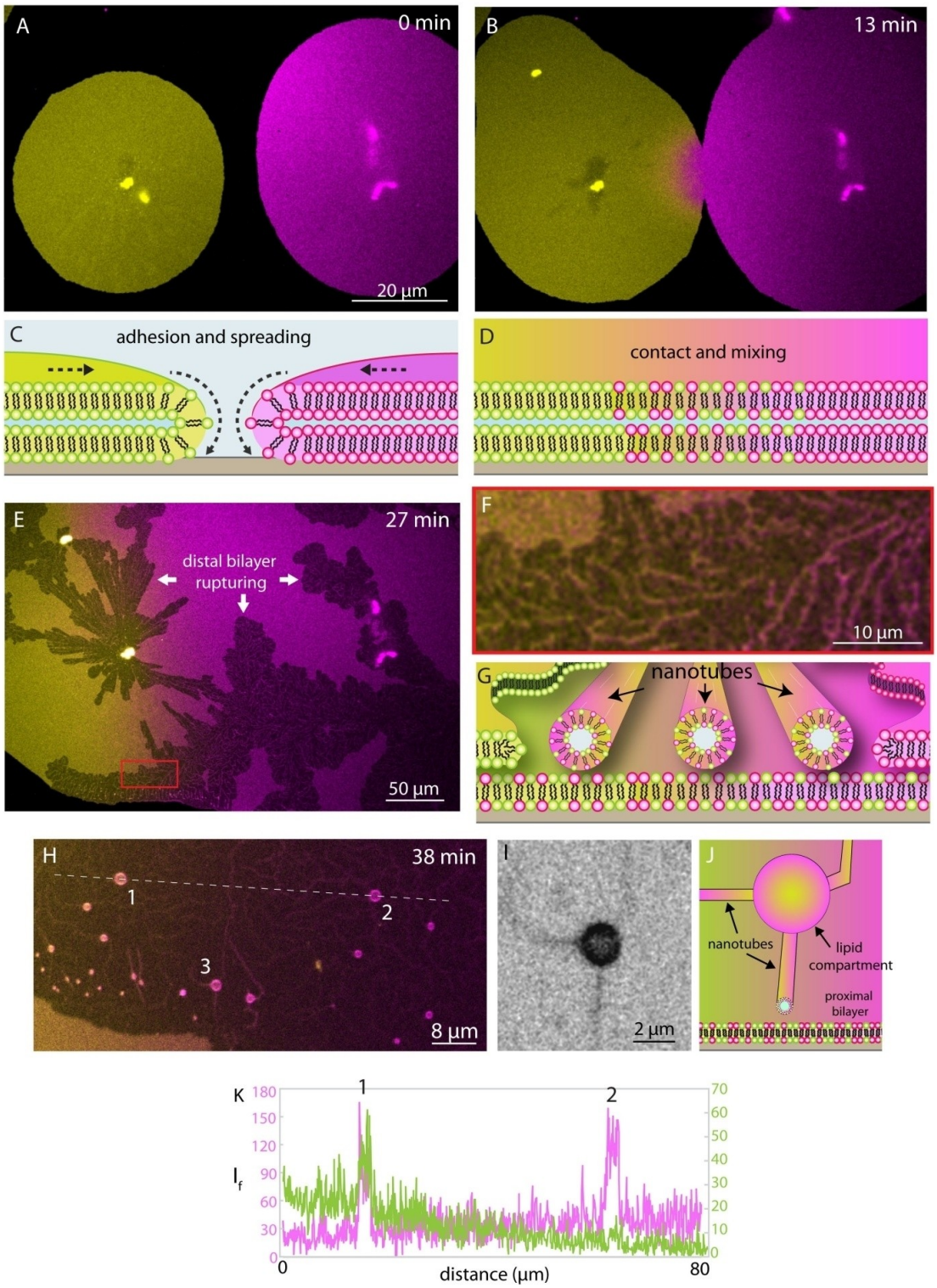

Figure 2. Fusion and mixing of spreading FGUVs. (A–B) Fluorescence microscopy images showing two advancing FGUVs, doped at 1 wt% with either CF 488-DOPE (yellow) or ATTO 655-DOPE (magenta) before (A) and after contact (B). (C–D) Corresponding graphics for (A) and (B), respectively, showing merging of the double bilayers and mixing of membrane lipids to produce a compositional gradient at the contact interface. (E) Fluorescence micrograph showing merged FGUVs with spontaneous rupturing of the distal bilayer during spreading. (F–G) Fluorescence micrograph (F) and graphical representation (G) showing transformation of the ruptured double bilayer into a network of lipid nanotubes (distal) supported on a surface-attached bilayer (proximal). (H–J) Emergence of spherical lipid compartments from lipid nanotube networks; fluorescence image showing three discrete lipid vesicles (#1,2,3) (H); magnified and inverted micrograph of a single vesicle (#3 in (H)) with nanotube connections (I); schematic drawing corresponding to the vesicle and nanotubes shown in (I) (J). (K) Fluorescence intensity profiles recorded along the white dashed line in (H). ATTO 655-DOPE (magenta plot); CF 488-DOPE (green plot). Labels 1 and 2 correspond to vesicles shown in (H). 1 wt% of fluorescent lipids were incorporated into the different MLV droplet reservoirs. Both fluorophores show comparable emission intensities in vesicle #1, due to the proximity to the contact interface and to energy transfer between the dyes (cf. discussion of Figure 4–5); in contrast, vesicle #2 is dominated by only one lipid due to negligible mixing of the advancing FGUVs. Imaging was performed with sequential scanning to ensure excitation of only one fluorophore at a time to minimize cross-talk. Micrographs show overlaid images of the two fluorescence channels.

the membranes of spherical vesicles are considered flat at the nanoscale; therefore there is no significant reduction in surface-free energy by merging of spherical GUVs. The interacting FGUVs continued to merge along the membrane interface to produce a single intact double-bilayered second generation flat protocell (SI Movie 1). After merging and further spreading of the fluorescent FGUVs, extensive regions of membrane rupture were observed in the distal lipid bilayer due to progressive increases in the membrane tension (Figure 2E, SI Movie 2).[4b,12] Rupture of the distal membrane gave rise to gradual de-wetting from the proximal membrane and formation of pores in the distal but not the proximal membrane, which remained intact as a supporting platform.[4b] Consequently, the remaining interconnections between the proximal and the distal membrane (pinning sites)[4b,13] were bounded by pores with increasing edge energy, such that the distal membrane fragments transformed into a proximal bilayer-supported network of interconnected nanotubes (Figure 2F–G).[12] The nanotubes are nonequlibrium membrane structures that form when a bilayer is pinned locally to the surface while retracting in the de-wetting process illustrated in Figure 2F.[12] Tube formation is also known to occur when a point force is applied to a flat membrane, e.g. the surface of a giant vesicle,[14] or in some instances when biological cells migrate on a surface.[15] The formation mechanism is similar to the instant transformation of small membrane patches into vesicles, owing to the competition between bending and edge energy.[16]

Over time (typically hours;[12] but only seconds if facilitated with temperature increase[17]), minimization of the membrane curvature and surface free energy resulted in transformation of the nanotubes into a population of micrometer-sized lipid vesicles that remain attached to the proximal lipid bilayer substrate (Figure 2H,I). Significantly, the vesicle buds were interconnected through an array of lipid nanotubes,[12,17–18] and were diverse in membrane composition depending on their location with respect to the contact interface (Figure 2J,K).

Artificial Predator-Prey Mechanism

We developed the above experiments to generate an artificial predator-prey mechanism between synthetic protocells.[19] To achieve this, we used two spreading FGUVs of disparate dimensions such that the smaller counterpart (prey protocell) was completely subsumed after collision and membrane fusion with the larger (predator) protocell. Upon contact and mixing, the fluorescence intensity of the prey FGUV decreased significantly as the associated fluorophore became depleted by infiltration of the membrane lipids of the predator protocell (Figures 3A–D, SI Movie 3). Similarly, the fluorescence intensity of the MLV of the prey FGUV progressively decreased after assimilation and subsequently adopted the fluorescence signature of the predator due to on-going lipid exchange that occurred without dissolution or rupturing of the reservoir microstructure. Time-dependent fluorescence intensity plots indicated that the fluorophore of the small FGUV was still detectable after several minutes of mixing (Figure 3E), indicating that although morphological features of the prey protocell were not incorporated into the predator FGUV, the latter displayed localized changes in composition. Consequently, subsequent rupturing of the distal lipid bilayer (SI Movie 4) in regions specifically associated with assimilation of the prey protocell gave rise to a localized population of vesicles with modified compositions (Figure 3F–H).

Compositional Diversity Across Protocell-Protocell Fusion Interfaces

To address the level of compositional diversity produced by spontaneous fusion of spreading FGUVs comprising different membrane lipids we analyzed the composition of 58 lipid vesicles that emerged in the ruptured lipid patches and displayed the ratios of the emissions emanating from the two fluorophores associated with the vesicles at three different consecutive time points (Figure 4A–D). At each time point, the intensity ratios revealed a distinct concentration gradient of both fluorophores over the entire lipid patch. The intensity ratios of both fluorophores were similar at the line of fusion, but with increasing distance (r) from the contact line the fluorophore intensities of the original FGUVs dominated. In each direction, there was a gradual decrease in the intensity of the invading fluorophore due to diffusive mixing of the spreading FGUVs. A quadratic function was used to fit the data points, assuming a $1/r^2$ dependence of the fluorophore concentration of the invading lipid FGUV and identical diffusive behavior of the two merging protocells. However, energy transfer from the blue-absorbing CF 488-DOPE (fluorophore A) to the red-absorbing ATTO 655-DOPE (fluorophore B) upon excitation decreased the fluorescence intensity (I_f) I_{fA}/I_{fB} ratio by an order of magnitude compared with I_{fB}/I_{fA}, with a concomitant decrease in the signal-to-noise ratio in the presence of the invading ATTO 655-DOPE-labelled FGUV (Figure 4D). Moreover, as prolonged rupturing of the distal bilayer often resulted in collapse or growth of the pre-existing vesicles and emergence of new vesicles during data collection (Figure 4E), an accurate quantitative determination of the spatiotemporal changes in the mixed lipid compositions was not possible. Similar experiments were undertaken on more complex interfaces, for example formed from the fusion of five FGUVs (SI Movie 5 and SI Section 2–3). Although qualitatively consistent, the studies indicated that the composition gradient was determined by the geometry of the contact interface, the ratio of the sizes of the merging FGUVs, and the number of FGUVs involved in the fusion process.

Having established the presence of a composition gradient in the vesicle population formed across the FGUV fusion interface, we employed a similar analysis of the lipid nanotube progenitors and their nearby regions of the proximal bilayer to ascertain the pathway responsible for the compositional diversity (Figure 5). Confocal fluorescence micrographs of ruptured membrane regions comprising networks of lipid nanotubes were used to determine the emission intensity ratios (I_{fA}/I_{fB} and I_{fB}/I_{fA}) in 36 different nanotubes and nearby areas of

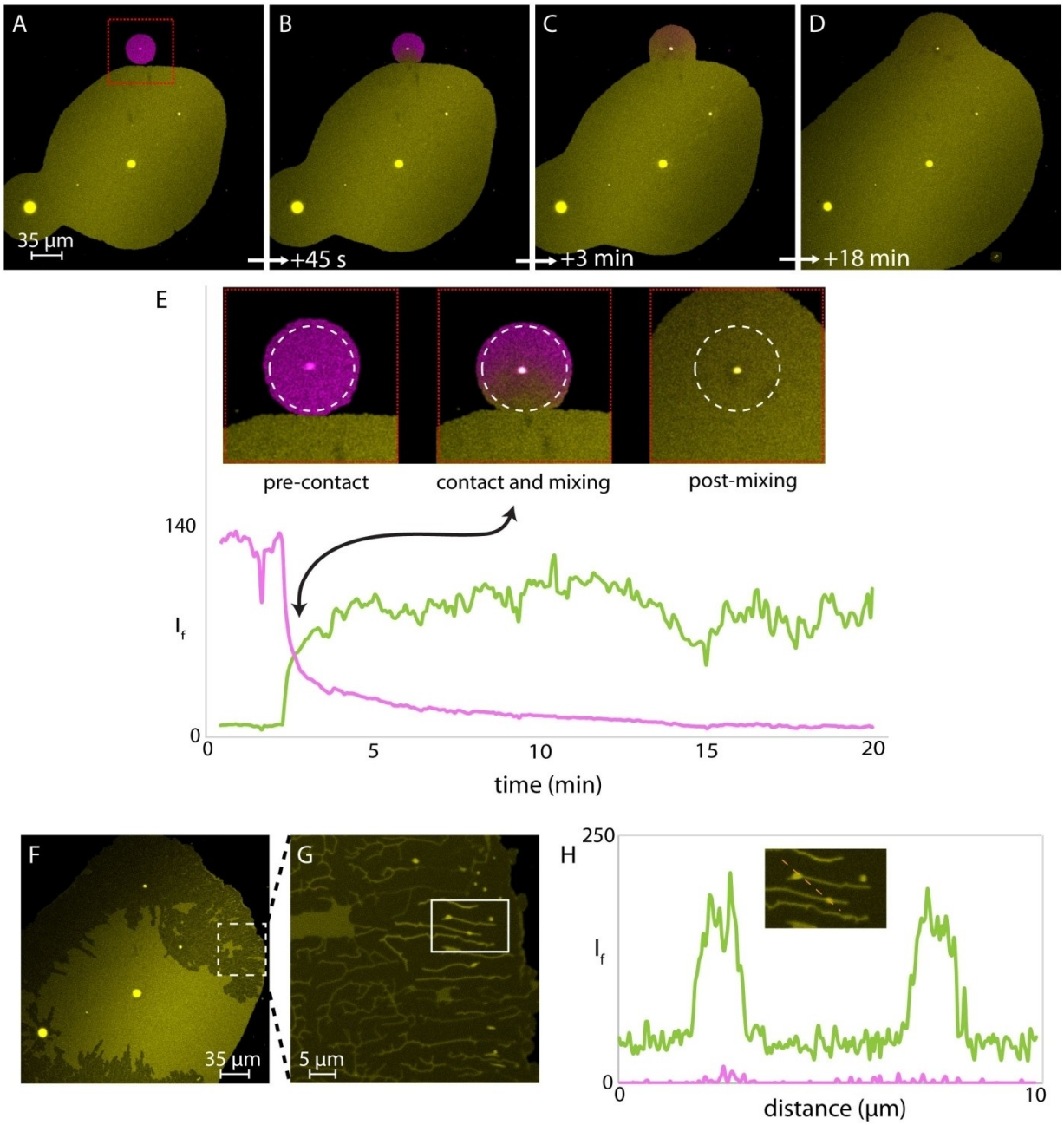

Figure 3. Predator-prey behavior among FGUVs. (A) Confocal fluorescence microscopy image showing two spreading FGUVs with disparate sizes before merging. The large and small FGUVs are labelled with CF 488-DOPE (yellow) and ATTO 655-DOPE (magenta) respectively. Small bright regions are the MLV reservoirs. (B–D) Time-series of fluorescence microscopy images showing that upon contact, the two FGUVs fuse and the small FGUV (prey protocell) is subsumed within the larger counterpart (predator protocell). (E) Time-dependent images and corresponding changes in the fluorescence intensities of ATTO 655-DOPE (magenta) and CF 488-DOPE (green) recorded within the prey FGUV (white dashed circle) during pre-contact, on contact, and after fusion and assimilation. (F–G) Morphological transformations in the resulting predator-prey protocell include rupturing of the distal lipid bilayer of the FGUV to generate a proximal bilayer-supported lipid nanotube network and discrete vesicles. (H) Fluorescence intensity profile recorded along the dashed red line shown in the inset (see also framed region in (G)). The low-level presence of 655-DOPE (magenta) from the subsumed prey protocell is observed along with CF 488-DOPE (green) from the predator FGUV.

the proximal bilayer (Figures 5A, C). The data showed that the I_{fA}/I_{fB} and I_{fB}/I_{fA} ratios increased at increasing distances from different sides of the fusion interface due to decreases in the concentrations of the invading lipids (Figures 5B, D), with ratios near 1.0 close to the contact interface. The data were consistent with the vesicle intensity analyses shown in Figure 4. However, I_{fA}/I_{fB} ratios recorded in regions away from the fusion interface and dominated by CF 488-DOPE (fluorophore A) were significantly lower in the lipid nanotubes compared with their adjacent proximal bilayers. In contrast, at the other side of the contact line where ATTO 655-DOPE (fluorophore B) dominated,

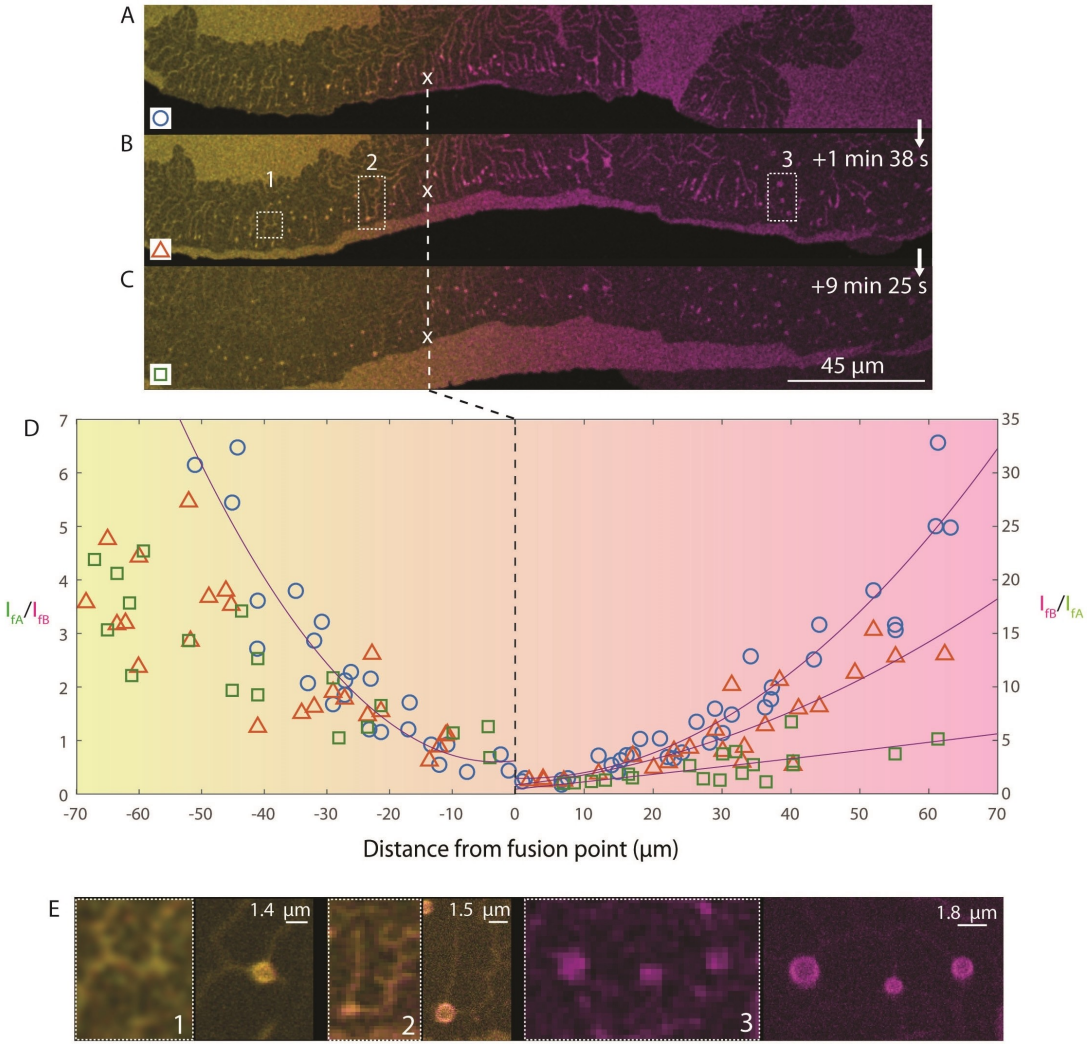

Figure 4. Compositional analyses of a vesicle population formed by merging and rupturing of two FGUVs at three different time points. (A–C) Confocal time series showing the same region on a rupturing lipid membrane produced by the merging of two different spreading FGUVs labelled with CF 488-DOPE (fluorophore A; yellow, left) and ATTO 655-DOPE (fluorophore B; magenta, right). Time points; *t* (A); *t* + 98 s (B); *t* + 565 s (C). The initial contact line between the two FGUVs is marked by a white cross/dashed line. (D) Graph showing the ratios of emission intensities from the lipid-conjugated fluorophores (I_{fA}/I_{fB} (left) and I_{fB}/I_{fA} (right) A = CF 488-DOPE, B = ATTO 655-DOPE) versus the distance from the fusion interface (black dashed line). Symbols (blue circle, red triangle, green square) correspond to data collected from the region shown in Figure 2E and at the different time points as displayed in (A–C). The I_{fA}/I_{fB} values are lower than I_{fB}/I_{fA} and display a lower signal-to-noise ratio especially at longer time intervals due to energy transfer from fluorophore A to fluorophore B upon excitation at 488 nm. The data points do not always represent the same vesicles among the three different time points due to vesicle instability or emergence of new lipid compartments. (E) Magnified confocal micrographs showing dynamics of vesicle production in areas of the ruptured membrane delineated by dashed boxes shown in panel B (regions; #1, #2, #3). Pairs of micrographs were taken 17, 14 and 8 minutes apart for regions #1, #2, #3, respectively. New vesicles emerge in regions #1 and #2, while pre-existing vesicles are observed to grow in #3).

the I_{fB}/I_{fA} ratios were higher in the nanotubes when compared to the nearby proximal bilayer regions.

The above results suggest that the rates of lipid mixing in the nanotubes and in the proximal bilayer are different after membrane rupture. Specifically, higher I_{fB}/I_{fA} ratios in the nanotubes in regions dominated by fluorophore B imply that the number of ATTO 655-DOPE lipids is higher in the distal bilayer-derived nanotubes than in the adjacent proximal bilayer. We attribute this to relatively fast rates of lipid mixing in the underlying bilayer until equilibration, compared with lower rates of lipid diffusion along the highly curved nanotubes. We postulate that the lipid flux to the nanotubes becomes limited as the counter-spreading FGUVs rupture. This implies that the nanotubes are physically connected to the proximal bilayer only through membrane defects,[5b] and that the fluorescence intensity ratios observed for the nanotubes represent lipid compositions of an earlier point in time and are spatiotemporally dependent. Consequently, close to the fusion interface between the two spreading FGUVs, a mixing ratio of ca. 1:1 is preserved as the final conditions are established at the onset of rupture. In contrast, at the other side of the contact interface where CF 488-DOPE fluorescence dominates, the lower I_{fA}/I_{fB} ratio determined in the nanotubes compared with nearby regions of the proximal bilayer may be due to differences in the extent of energy transfer from blue-absorbing CF 488-DOPE to red-absorbing ATTO 655-DOPE. In particular, the supply of new

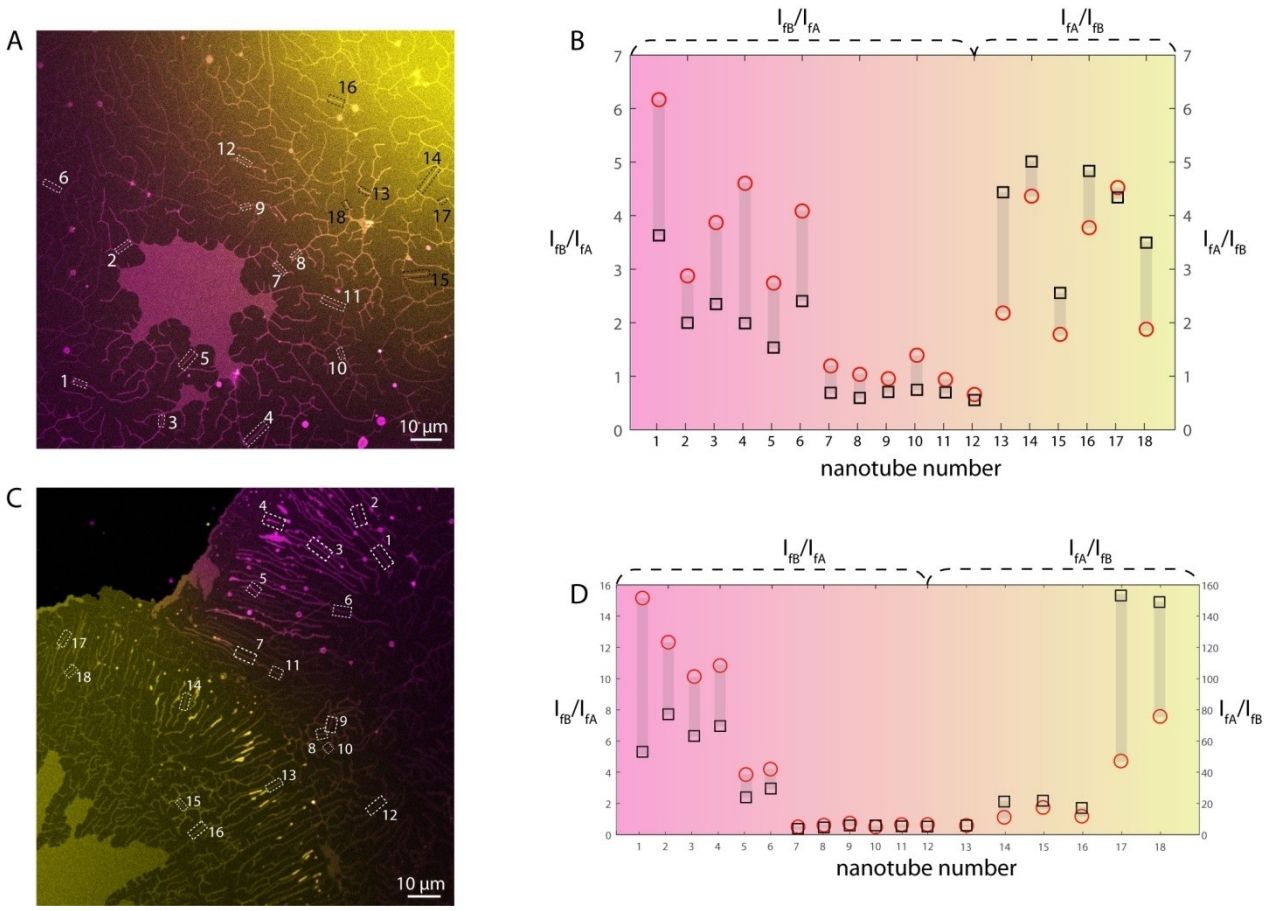

Figure 5. Compositional analyses of lipid nanotubes and the proximal bilayer of the ruptured FGUV. (A, C) Confocal micrographs of two different ruptured membrane regions with a network of lipid nanotubes. Both fluorophores are visible in the micrograph indicating fusion and mixing in the imaged region at an earlier point in time. (B, D) Graphs showing the intensity ratios of ATTO 655-DOPE (fluorophore B; magenta), CF 488-DOPE (fluorophore A; yellow) fluorescence (I_{fB}/I_{fA}, left *y* axis) and I_{fA}/I_{fB} (right *y* axis) for a total of 18 nanotubes per experiment. The nanotubes and the proximal bilayer regions in the vicinity of each nanotube are framed in dashed lines in (A) and (C). Intensity ratio data for the nanotubes (red circles) and nearby proximal bilayer of each nanotube (black squares) are shown at a single time point. Each number on the x-axis in B and D corresponds to the same number label associated with the nanotubes shown in A and C. Light gray stripes in B and D connect the pairing of data markers for each nanotube and its associated proximal membrane region.

fluorophore A lipids required to replenish the CF 488-DOPE intensity loss would be curtailed by the lower rates of lipid diffusion into the nanotubes while more efficient mixing in the proximal bilayer provides a continuous supply of CF 488-DOPE. Consequently, the loss of fluorescence intensity of fluorophore A to fluorophore B in the proximal membrane is compensated by the continuous supply of new lipids carrying fluorophore A. The impact of the energy transfer therefore would be less significant in the proximal membrane than in the nanotubes, resulting in higher I_{fA}/I_{fB} values in the planar membrane than in the lipid nanotubes. Moreover, CF 488-DOPE has a lower excitation wavelength and is less photostable than ATTO 655-DOPE, and therefore subject to increased levels of photobleaching, particularly in the nanotubes which are only slowly replenished with new lipid molecules.

Discussion

In this work we describe a spontaneous pathway to compositional diversity in model protocells that incorporates the spreading and merging of FGUVs with different membrane compositions followed by post-fusion structural reconfiguration into interconnected networks of third-generation lipid vesicles. The combination of fusion and wetting/rupturing converts continuous flat lipid vesicles into populations of discrete spherical vesicles with membrane compositions that are spatiotemporally inherited across the fusion interface. Formation and rupture of the FGUVs is an autonomous process that is primarily dependent on the type of wetting interactions with the solid surface. Fusion and mixing of the membrane lipids are energetically favorable due to the high curvature circumference of the FGUVs, and diffusion limitations across the fusion interface give rise to compositional gradients that are maintained over sufficiently long periods of time that a progeny vesicle population with inherited compositions grows by localized swelling of the nanotube network. As lipid mixing

occurs at different rates on the distal and proximal bilayers due to rupturing in the distal bilayer that interrupts diffusive flow, lipid exchange between the distal and proximal bilayer occurs slowly through handle pores at rates similar to the diffusion through the nanotube network.[5b] Thus, the composition gradient of the nanotube network and attached next-generation lipid vesicles only change slowly in contrast to the relatively rapid mixing in the proximal bilayer. Indeed, once the vesicles are formed in the network nodes, their membrane composition is only slowly altered by the inflow of lipids from remote areas.

We speculate that our flat protocell model could contribute a surface-supported self-optimization pathway to the emergence of compositionally diverse sets of protocells on the early Earth. Firstly, FGUVs are directly derived from MLVs which are the result of dehydration-rehydration of lipid layers,[20] similar to the dry-wet cycles invoked in the hot spring hypothesis of the origin of life.[21] Secondly, the morphological, dynamical and reconfiguration properties of FGUVs are dependent on mineral surface-supported processes that mechanistically provide a geochemical context for the stabilization, physical evolution and dispersion of primitive cells on the early Earth. Thirdly, the intrinsic instability of the distal bilayer of the merged FGUVs produces next-generation vesicles that become disconnected and eventually detach from the nanotube network,[12] suggesting a plausible pathway to the continuous dispersion of compositionally variant protocells into the geochemical environment. Finally, although fusion events associated with the merging of FGUVs with similar compositions and highly mismatched dimensions give rise to dissipation of the prey protocells within the membrane of the predator protocell, in principle, using prey protocells comprising lipids that have low solubility in the predator matrix could provide isolated compositional patches within the spreading predatory FGUV. Thus, rudimentary predator-prey behavior could provide a mechanism for the development of compositional "mutations" in a sub-set of progeny vesicles. Such marked alterations in the inherited mechanical stability, membrane fluidity, membrane domains and molecular-selective permeability of the vesicles could generate isolated membrane domains required for the emergence of membrane protein organization and associated functions such as transmembrane signaling and osmotic relaxation[22,23].

Supporting Information

The authors have cited additional references within the Supporting Information.[24,25]

Acknowledgements

This work was made possible through financial support obtained from the Research Council of Norway (Norges Forskningsråd) Project Grant 324630. S.M. was funded by the ERC Advanced Grant Scheme (EC-2016-674 ADG 740235). AJ acknowledges funding by the European Union Marie Skłodowska-Curie Actions program, grant ID 812868 and the European Union Excellent Science – Future and Emerging Technologies (FET) program, grant ID 899205.

Conflict of Interests

The authors declare no conflict of interest.

Data Availability Statement

The data that support the findings of this study are available from the corresponding author upon reasonable request.

Keywords: protocell · diversity · abiogenesis · lipid · vesicle

[1] a) D. A. Baum, *Bioscience* **2015**, *65*, 678–684; b) T. Z. Jia, M. Caudan, I. Mamajanov, *Life* **2021**, *11*, 154; c) K. Ruiz-Mirazo, C. Briones, A. de la Escosura, *Open Biol.* **2017**, *7*, 170050.
[2] T. West, V. Sojo, A. Pomiankowski, N. Lane, *Philos. Trans. R. Soc. London Ser. B* **2017**, *372*, 20160419.
[3] A. Ianeselli, D. Tetiker, J. Stein, A. Kühnlein, C. B. Mast, D. Braun, T. Y. D. Tang, *Nat. Chem.* **2022**, *14*, 32–39.
[4] a) I. Gözen, *The self-spreading double bilayer – Advances in lipid membrane nanotechnology* (Göteborg), **2013**; b) I. Gözen, P. Dommersnes, I. Czolkos, A. Jesorka, T. Lobovkina, O. Orwar, *Nat. Mater.* **2010**, *9*, 908–912; c) T. Lobovkina, I. Gözen, Y. Erkan, J. Olofsson, S. G. Weber, O. Orwar, *Soft Matter* **2010**, *6*, 268–272; d) I. Gözen, M. Shaali, A. Ainla, B. Örtmen, I. Põldsalu, K. Kustanovich, G. D. M. Jeffries, Z. Konkoli, P. Dommersnes, A. Jesorka, *Lab Chip* **2013**, *13*, 3822–3826.
[5] a) J. Leng, F. Nallet, D. Roux, *Eur. Phys. J. E* **2001**, *4*, 77–83; b) I. Gozen, P. Dommersnes, O. Orwar, A. Jesorka, *Soft Matter* **2012**, *8*, 6220–6225.
[6] I. Gözen, C. Billerit, P. Dommersnes, A. Jesorka, O. Orwar, *Soft Matter* **2011**, *7*, 9706–9713.
[7] R. L. Schoch, I. Barel, F. L. H. Brown, G. Haran, *J. Chem. Phys.* **2018**, *148*, 123333.
[8] a) T. Litschel, P. Schwille, in *Annual Review of Biophysics, Vol. 50*, Annual Reviews, **2021**, pp. 525–548; b) V. Mukwaya, S. Mann, H. Dou, *Commun. Chem.* **2021**, *4*.
[9] a) T. Bilal, I. Gözen, *Biomater. Sci.* **2017**, *5*, 1256–1264; b) E. S. Köksal, P. F. Belletati, G. Reint, R. Olsson, K. D. Leitl, I. Kantarci, I. Gözen, *JoVE* **2019**, e58923.
[10] a) K. Spustova, E. S. Köksal, A. Ainla, I. Gözen, *Small* **2021**, *17*, 2005320; b) C. Katke, E. Pedrueza-Villalmanzo, K. Spustova, R. Ryskulov, C. N. Kaplan, I. Gözen, *ACS Nano* **2023**, *17*, 3368–3382.
[11] J. Raedler, H. Strey, E. Sackmann, *Langmuir* **1995**, *11*, 4539–4548.
[12] E. S. Köksal, S. Liese, I. Kantarci, R. Olsson, A. Carlson, I. Gözen, *ACS Nano* **2019**.
[13] a) M. Taylor, I. Gözen, S. Patel, A. Jesorka, K. Bertoldi, *PLoS One* **2016**, *11*, e0165947; b) A. Gupta, I. Gözen, M. Taylor, *Soft Matter* **2019**, *15*, 4178–4186.
[14] A. Jesorka, N. Stepanyants, H. Zhang, B. Ortmen, B. Hakonen, O. Orwar, *Nat. Protoc.* **2011**, *6*, 791–805.
[15] S. Yu, L. Yu, *FEBS J.* **2022**, *289*, 7246–7254.
[16] C. Has, S. Pan, *J. Liposome Res.* **2021**, *31*, 90–111.
[17] E. S. Köksal, S. Liese, L. Xue, R. Ryskulov, L. Viitala, A. Carlson, I. Gözen, *Small* **2020**, *16*.
[18] a) I. J. Schanke, L. Xue, K. Spustova, I. Gözen, *Nanoscale* **2022**, *14*, 10418–10427; b) E. S. Köksal, I. Põldsalu, H. Friis, S. J. Mojzsis, M. Bizzarro, I. Gözen, *ChemSystemsChem* **2022**, *4*, e202100040; c) I. Põldsalu, E. S. Köksal, I. Gözen, *Phys. Chem. Chem. Phys.* **2021**, 26948–26954.
[19] a) Y. Qiao, M. Li, R. Booth, S. Mann, *Nat. Chem.* **2017**, *9*, 110–119; b) L. Rodríguez-Arco, M. Li, S. Mann, *Nat. Mater.* **2017**, *16*, 857–863; c) Y. Qiao, M. Li, D. Qiu, S. Mann, *Angew. Chem. Int. Ed.* **2019**, *58*, 17758–17763.

[20] a) I. Gözen, E. S. Köksal, I. Põldsalu, L. Xue, K. Spustova, E. Pedrueza-Villalmanzo, R. Ryskulov, F. Meng, A. Jesorka, *Small* **2022**, *18*; b) A. Lopez, M. Fiore, *Life (Basel)* **2019**, *9*.
[21] B. Damer, D. Deamer, *Astrobiology* **2019**, *20*, 429–452.
[22] a) M. A. Lemmon, *Nat. Rev. Mol. Cell Biol.* **2008**, *9*, 99–111; b) S. Sonnino, A. Prinetti, *Curr. Med. Chem.* **2013**, *20*, 4–21.
[23] K. Oglęcka, P. Rangamani, B. Liedberg, R. S. Kraut, A. N. Parikh, *eLife* **2014**, *3*, e03695.
[24] M. Karlsson, K. Nolkrantz, M. J. Davidson, A. Strömberg, F. Ryttsén, B. Åkerman, O. Orwar, *Anal. Chem.* **2000**, *72*, 5857–5862.
[25] a) T. Bilal, I. Gözen, *Biomater. Sci.* **2017**, *5*, 1256–1264; b) T. Lobovkina, P. Dommersnes, J.-F. Joanny, J. Hurtig, O. Orwar, *Phys. Rev. Lett.* **2006**, *97*, 188105.

Manuscript received: March 24, 2024
Accepted manuscript online: May 12, 2024
Version of record online: ■■, ■■

RESEARCH ARTICLE

We present a feasible pathway leading to a rudimentary type of protocell diversity and speciation based on the fusion of flat giant unilamellar lipid vesicles on solid surfaces.

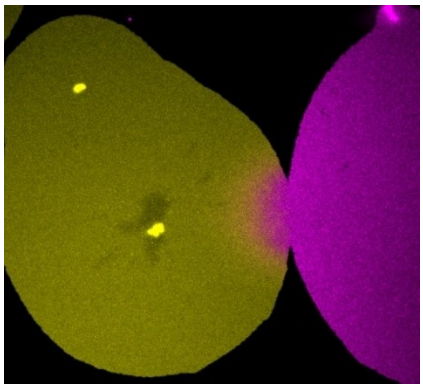

Dr. İ. Gözen, Prof. S. Mann, Prof. A. Jesorka*